Crystal Calorimeters in the Next Decade

Ren-Yuan Zhu, *Senior Member, IEEE*

***Abstract*—Crystal calorimeter has traditionally played an important role in precision measurement of electrons and photons in high energy physics experiments. Recent interest in calorimeter technology extends its application to measurement of hadrons and jets with dual readout. Potential application of new generation scintillating crystals of high density and high light yield, such as LYSO, in high energy physics experiments is described. Candidate crystals for the homogeneous hadronic calorimeter concept are also discussed.**

***Index Terms*—Crystal; Scintillator; Calorimeter; Dual Readout; Homogeneous Hadronic Calorimeter.**

I. Introduction

Octal absorption shower counters made of inorganic crystal scintillators have been known for decades for their superb energy resolution and detection efficiency [1]. In high energy and nuclear physics, crystal calorimeters have been constructed, and their use has been a key factor in the successful physics programs of many experiments. The physics discovery potential of crystal calorimeter was early demonstrated by the Crystal Ball experiment through its study of radiative transitions and decays of the Charmonium family [2]. Figure 1 (Left) shows nearly all the principal radiative transition lines of the Charmonium system simultaneously measured by the NaI(Tl) crystal calorimeter.

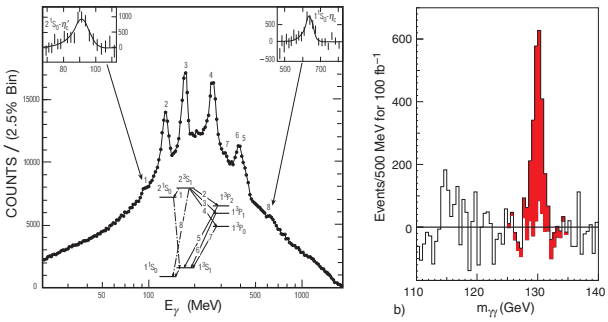

Fig. 1. Left: An inclusive photon spectrum measured at the ψ' by the NaI(Tl) crystal calorimeter of the Crystal Ball experiment at SLAC [2]. Right: The expected background subtracted Higgs mass peak reconstructed from its two photon decays measured by the CMS $PbWO_4$ crystal calorimeter [3].

The designed goal of the CMS lead tungstate ($PbWO_4$) crystal calorimeter [3] is to maximize its physics discovery potential in searching for narrow resonances in photon and electron final states at LHC. Figure 1 (Right) shows the expected background subtracted Higgs peak reconstructed with its two decay photons by the CMS $PbWO_4$ calorimeter. The ability of the Higgs discovery via this decay channel is directly related to the energy resolution of the calorimeter.

This work was supported in part by the U.S. Department of Energy under grant DE-FG03-92-ER-40701 and the U.S. National Science Foundation Award PHY-0612805.

The authors are with the California Institute of Technology, Pasadena, CA 91125 USA (e-mail:zhu@hep.caltech.edu).

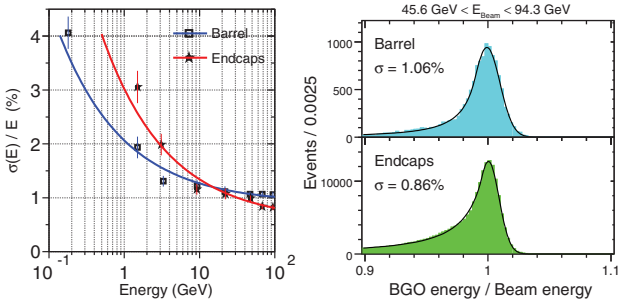

Fig. 2. Left: The energy resolution of the L3 BGO calorimeter as a function of electron energy measured in the CERN test beam. Right: The energy resolution of Bhabha electrons observed by the L3 BGO calorimeter *in situ* at LEP by using the RFQ calibration.

Crystal calorimeters have been constructed, and their use has been a key factor in the successful physics programs of many experiments. With proper calibration and monitoring, crystal calorimeters usually achieve their designed resolution *in situ* [4]. Figure 2 (Left) shows energy resolution as a function of the electron energy obtained with the L3 BGO calorimeter in the CERN test beam, which is in a good agreement with the resolution of Bhabha electrons reconstructed *in situ* at LEP, as shown in Figure 2 (Right). To achieve this resolution a radio frequency quadrupole accelerator based calibration technique was used [5].

Table I summarizes parameters of past and present crystal calorimeters in high energy physics. One notes that each of these calorimeters requires several cubic meters of high quality crystals. The most ambitious crystal calorimeter in Table I is presumably the CMS calorimeter which uses 11 m^3 $PbWO_4$ crystals. Its designed energy resolution [3] is

$$\sigma_E/E = \mathbf{2.7\%}/\sqrt{E} \oplus \mathbf{0.55\%} \oplus 0.16/E \qquad (1)$$

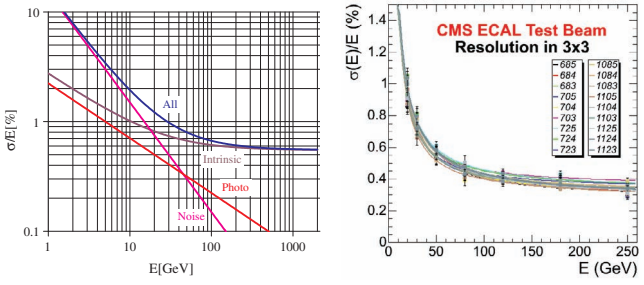

Fig. 3. Left: The designed energy resolution of the CMS $PbWO_4$ calorimeter and corresponding contributions is shown as a function of energy [3]. Right: The energy resolution of two groups of 9 $PbWO_4$ crystals is shown as function of electron energy obtained in the CMS ECAL beam test [6].

TABLE I
CRYSTAL CALORIMETER IN HIGH ENERGY PHYSICS: PAST AND PRESENT

Experiment	C. Ball	L3	CLEO II	KTeV	*BaBar*	BELLE	CMS
Accelerator	SPEAR	LEP	CESR	Tevatron	PEP II	KEK	LHC
Date	75–85	80–00	80–00	90–10	94–10	94–10	95–20
Crystal Type	NaI(Tl)	BGO	CsI(Tl)	CsI	CsI(Tl)	CsI(Tl)	$PbWO_4$
B-Field (Tesla)	-	0.5	1.5	-	1.5	1.0	4.0
Inner Radius (m)	0.254	0.55	1.0	-	1.0	1.25	1.29
Number of Crystals	672	11,400	7,800	3,300	6,580	8,800	76,000
Crystal Depth (X_0)	16	22	16	27	16 to 17.5	16.2	25
Crystal Volume (m^3)	1	1.5	7	2	5.9	9.5	11
L. Yield (p.e./MeV)	350	1,400	5,000	40	5,000	5,000	2
Photo-sensor	PMT	Si PD	Si PD	PMT	Si PD	Si PD	APD†
Photo-sensor Gain	Large	1	1	4,000	1	1	50
Noise/Can. (MeV)	0.05	0.8	0.5	Small	0.15	0.2	30
Dynamic Range	10^4	10^5	10^4	10^4	10^4	10^4	10^5

† Avalanche photo-diode.

for the barrel, and

$$\sigma_E/E = \mathbf{5.7\%}/\sqrt{E} \oplus \mathbf{0.55\%} \oplus 0.77/E \qquad (2)$$

for the endcaps.

Figure 3 (Left) shows the designed energy resolution as a function of energy for the CMS $PbWO_4$ calorimeter. It can be decomposed to three contributions from photo-electron statistics (stochastic), intrinsic shower leakage (stochastic and constant) and readout noise (noise). Figure 3 (Right) shows the energy resolution as a function of electron energy measured in the CERN test beam for two groups of 3×3 crystals, independent of their impact position on the crystal front face [6]. The measured resolution in the low and middle energy region agrees well with the designed resolution. At the high energy region, the measured energy resolution is better than the design values since there is no calibration uncertainty in the test beam data.

Recent interest in homogeneous crystal hadronic calorimeter extends its application to measurement of hadrons and jets with high resolution [7]. This detector concept adapts dual readout for both Cherenkov and scintillation light, which is extensively studied recently by the Dream collaboration [8].

Section II of this paper describes optical and scintillation properties of heavy crystal scintillators commonly used in particle physics experiment. Fast and bright crystals discovered in the last two decades, such as cerium doped lutetium oxyorthosilicate ($Lu_2(SiO_4)O$ or LSO) [9], cerium doped lutetium yttrium oxyorthosilicate ($Lu_{2(1-x)}Y_{2x}SiO_5$, LYSO) [10] and cerium doped lanthanum tri-halides,e.g. $LaCl_3$ and $LaBr_3$[11] are also covered. The expected performance of a LYSO electromagnetic calorimeter is elaborated in Section III. Section IV discusses candidate crystals for the homogeneous crystal hadronic calorimeter concept.

II. PROPERTIES OF CRYSTAL SCINTILLATORS

Table II lists basic properties of heavy crystals with mass production capability: NaI(Tl), CsI(Tl), BaF_2, CeF_3, bismuth gemanade ($Bi_4Ge_3O_{12}$ or BGO), lead tungstate ($PbWO_4$ or PWO), LSO/LYSO [12] and PbF_2. All, except PbF_2, are scintillators with the characteristics of their scintillation light listed. All, except CeF_3, have either been used in, or actively pursued for, high energy and nuclear physics experiments, which are also listed in the table. The experiment name in bold indicates the future crystal calorimeters in the next decade. LSO and LYSO crystals are also widely used in the medical industry. Mass production capabilities exist for all these crystals.

Figure 4 is a photo showing twelve crystal scintillator samples. In addition to samples listed in Table II pure CsI, CsI(Na), LYSO as well as $LaCl_3$ and $LaBr_3$ are also shown in this photo although the last two are not yet in mass production stage. Samples are arranged in an order of their density, or radiation length. All non-hygroscopic samples are wrapped with white Tyvek paper as reflector. Hygroscopic NaI, CsI, $LaBr_3$ and $LaCl_3$ are sealed in package with two ends made of quartz windows of 3 or 5 mm thick to avoid surface degradation. To minimize uncertainties in light output measurement caused by the sample size dependence all samples have a cubic shape of $1.5 \times 1.5 \times 1.5$ X_0^3, except NaI(Tl) and $LaCl_3$ which are a cylinder with a length of 1.5 X_0 and areas at two ends equaling to 1.5×1.5 X_0^2 to match the 2 inch diameter of the PMT cathode.

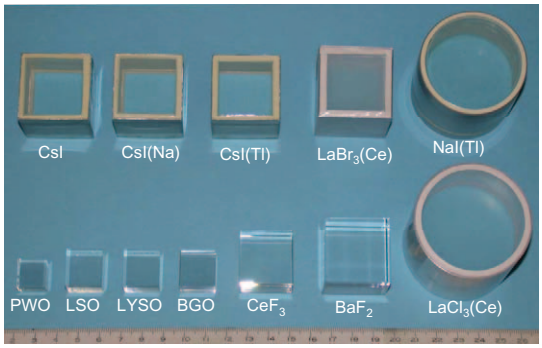

Fig. 4. A photo shows twelve crystal scintillators with dimension of 1.5 X_0.

TABLE II
PROPERTIES OF HEAVY CRYSTAL WITH MASS PRODUCTION CAPABILITY

Crystal	NaI(Tl)	CsI(Tl)	BaF_2	CeF_3	BGO	$PbWO_4$	LSO(Ce)	PbF_2
Density (g/cm^3)	3.67	4.51	4.89	6.16	7.13	8.3	7.40	7.77
Melting Point (°C)	651	621	1280	1460	1050	1123	2050	824
Radiation Length (cm)	2.59	1.86	2.03	1.70	1.12	0.89	1.14	0.93
Molière Radius (cm)	4.13	3.57	3.10	2.41	2.23	2.00	2.07	2.21
Interaction Length (cm)	42.9	39.3	30.7	23.2	22.7	20.7	20.9	21.0
Refractive Index[a]	1.85	1.79	1.50	1.62	2.15	2.20	1.82	1.82
Hygroscopicity	Yes	Slight	No	No	No	No	No	No
Luminescence[b] (nm)	410	560	300	340	480	425	420	?
(at Peak)			220	300		420		
Decay Time[b] (ns)	245	1220	650	30	300	30	40	?
			0.9			10		
Light Yield[b,c]	100	165	36	7.3	21	0.30	85	?
			4.1			0.077		
d(LY)/dT[b,d] (%/°C)	-0.2	0.4	-1.9	∼0	-0.9	-2.5	-0.2	?
			0.1					
Experiment	Crystal	CLEO	TAPS	-	L3	CMS	**SuperB**	A4
	Ball	*BaBar*			BELLE	ALICE	**KLOE-2**	**HHCAL?**
		BELLE				PrimEx	**SLHC?**	
		BES III				**Panda**		

a At the wavelength of the emission maximum.
b Top line: slow component, bottom line: fast component.
c Relative light yield of samples of 1.5 X_0 and with the PMT quantum efficiency taken out.
d At room temperature.

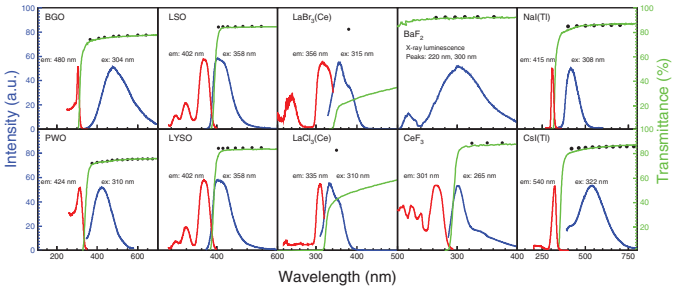

Fig. 5. The excitation (red) and emission (blue) spectra (left scale) and the transmittance (green) spectra (right scale) are shown as a function of wavelength for ten crystal scintillators. The solid black dots are the theoretical limit of the transmittance.

Figure 5 shows a comparison of the transmittance, emission and excitation spectra as a function of wavelength for ten samples. The solid black dots in these plots are the theoretical limit of the transmittance, which was calculated by using corresponding refractive index as a function of wavelength taking into account multiple bounces between the two parallel end surfaces and assuming no internal absorption [13]. Most samples, except $LaBr_3$ and $LaCl_3$, have their transmittance approaching the theoretical limits, indicating negligible internal absorption. The poor transmittance measured for $LaBr_3$ and $LaCl_3$ samples is probably due to scattering centers inside these samples.

It is interesting to note that BaF_2, BGO, NaI(Tl), CsI(Tl) and $PbWO_4$ have their emission spectra well within the transparent region showing no obvious self-absorption effect. The UV absorption edge in the transmittance spectra of LSO, LYSO, CeF_3, $LaBr_3$ and $LaCl_3$, however, cuts into the emission spectra and thus affects crystal's light output. This self-absorption effect is more seriously in long crystal samples used in high energy and nuclear physics experiment as extensively discussed for LSO and LYSO crystals [14].

Figure 6 shows the ^{137}Cs γ-ray pulse hight spectra measured by a Hamamatsu R1306 PMT with bi-alkali cathode for twelve crystal samples. Also shown in these figures are the corresponding FWHM energy resolution (E.R.). γ-ray spectroscopy with a few percents resolution is required to identify isotopes for the homeland security applications. It is clear that only $LaBr_3$ approaches this requirement. All other crystals do not provide sufficient energy resolution at low energies.

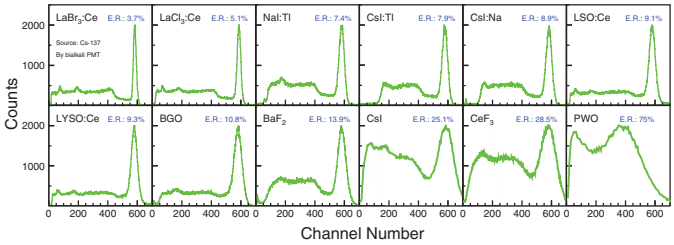

Fig. 6. ^{137}Cs γ-ray pulse hight spectra measured by a Hamamatsu R1306 PMT are shown for twelve crystal samples. The numerical values of the FWHM resolution (E.R.) are also shown in the figure.

Figure 7 shows light output in photo-electrons per MeV energy deposition as a function of the integration time, measured by using a Photonis XP2254b PMT with multi-alkali photo cathode, for six fast crystal scintillators (Left): $LaBr_3$, LSO, LYSO, CeF_3, un-doped CsI and $PbWO_4$ and six slow

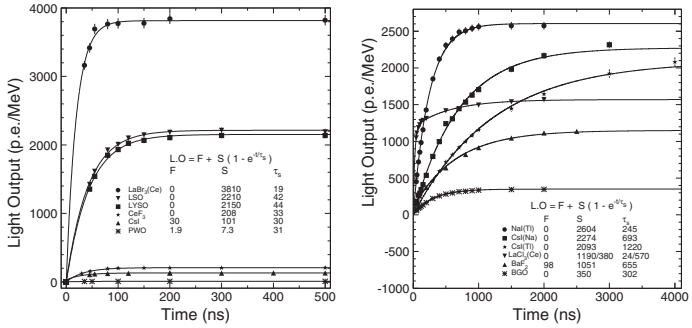

Fig. 7. Light output measured by using a XP2254b PMT is shown as a function of integration time for six fast (Left) and six slow (Right) crystal scintillators.

crystal scintillators (Right): NaI(Tl), CsI(Na), CsI(Tl), $LaCl_3$, BaF_2 and BGO. The corresponding fits to the exponentials and their numerical results are also shown in these figures. The un-doped CsI, $PbWO_4$, $LaCl_3$ and BaF_2 crystals are observed to have two decay components. Despite its poor transmittance the cerium doped $LaBr_3$ is noticed by its bright fast scintillation, leading to the excellent energy resolution for the γ-ray spectroscopic applications. The LSO and LYSO samples have consistent fast decay time ($\sim$40 ns) and photo-electron yield, which is 6 and 230 times of BGO and $PbWO_4$ respectively.

TABLE III
EMISSION WEIGHTED QUANTUM EFFICIENCIES (%)

Emission	LSO/LYSO	BGO	CsI(Tl)
Hamamatsu R1306 PMT	12.9±0.6	8.0±0.4	5.0±0.3
Hamamatsu R2059 PMT	13.6±0.7	8.0±0.4	5.0±0.3
Photonis XP2254b	7.2±0.4	4.7±0.2	3.5±0.2
Hamamatsu S2744 PD	59±4	75±4	80±4
Hamamatsu S8664 APD	75±4	82±4	84±4

Since the quantum efficiency of the PMT used for the light output measurement is a function of wavelength, it should be taken out to directly compare crystal's light output. Figure 8 shows typical quantum efficiency as a function of wavelength for a PMT with bi-alkali cathode (Hamamatsu R1306) and a PMT with multi-alkali cathode (Photonis 2254B), a Si APD (Hamamatsu S8664) and a Si PIN PD (Hamamatsu S2744). The emission spectra of LSO/LYSO, BGO and CsI(Tl) crystals are also shown in these figures. Table III summarized numerical result of the emission weighted average quantum efficiency for several readout devices. The light output values in Table II are listed with the PMT quantum efficiency taken out. The light output of LSO and LYSO crystals is a factor of 4 and 200 of that of BGO and $PbWO_4$ respectively.

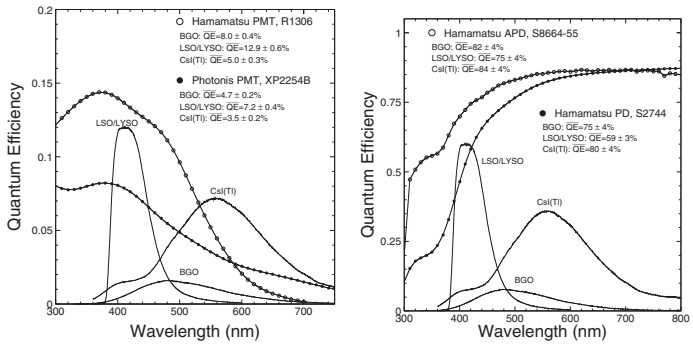

Fig. 8. Left: Quantum efficiencies of a Hamamatsu 1306 PMT with bi-alkali cathode (open circles) and a Photonis 2254B PMT with multi-alkali cathode (solid dots) are shown as a function of wavelength together with the emission spectra of the LSO/LYSO, BGO and CsI(Tl) samples, where the area under the emission curves is proportional to their corresponding absolute light output. Right: The same for a Hamamatsu S8664 Si APD (open circles) and a Hamamatsu S2744 Si PIN diode (solid dots).

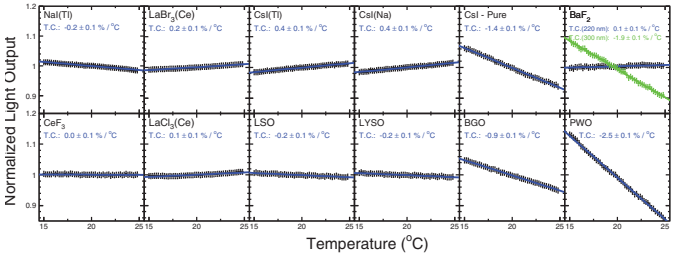

Fig. 9. Light output temperature coefficient obtained from linear fits between 15°C and 25°C for twelve crystal scintillators.

Scintillation light yield of crystals may also depends on the temperature. Fig 9 shows light output variations for twelve crystal samples between 15°C and 25°C. The corresponding temperature coefficients obtained from linear fits are also listed in the figure. The numerical result of these fits is also listed in Table II.

III. LYSO CRYSTAL ELECTROMAGNETIC CALORIMETER

Because of their board application in medical industry large size LSO and LYSO crystals with consistent optical and scintillation properties have been routinely grown [14]. Figure 10 shows four long crystal samples of $2.5 \times 2.5 \times 20$ cm^3. Figure 11 shows the spectra of 0.51 MeV γ-rays from a ^{22}Na source observed with coincidence triggers [14]. The readout devices used are a Hamamatsu R1306 PMT (Left) and 2 Hamamatsu S8664-55 APDs (Right). The FWHM resolution for the 0.51 MeV γ-ray with the PMT readout is about 12% to 13% for these long samples, which can be compared to 15%

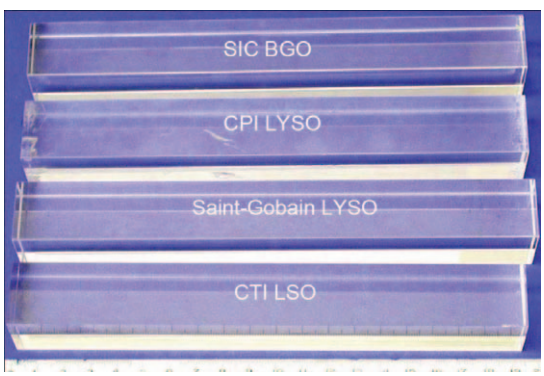

Fig. 10. A photo shows four long crystal samples with dimension of $2.5 \times 2.5 \times 20$ cm^3.

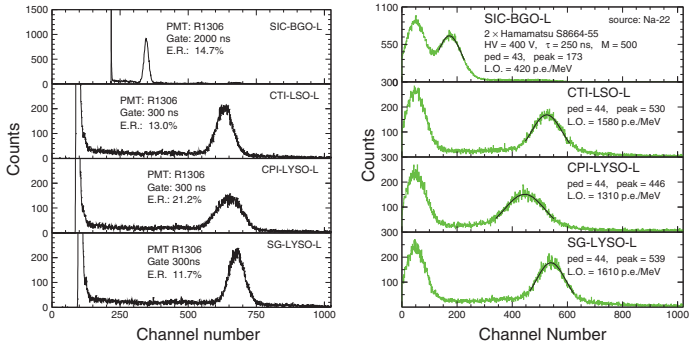

Fig. 11. The 0.511 MeV γ-rays spectra from a ^{22}Na source measured with a coincidence trigger using a Hamamatsu R1306 PMT (Left) and two Hamamatsu S8664-55 APDs (Right) for long BGO, LSO and LYSO samples of $2.5 \times 2.5 \times 20$ cm^3 size.

for the BGO sample. With APD readout, the γ-ray peaks are clearly visible. The energy equivalent readout noise was less than 40 keV for these long LSO and LYSO samples.

LSO/LYSO crystals is also found to be much more radiation hard than other crystals commonly used in high energy and nuclear physics experiment, such as BGO, CsI(Tl) and $PbWO_4$ [15]. Their scintillation mechanism is not damaged by γ-ray irradiation. Radiation damage in LSO and LYSO crystals recovers very slow under room temperature but can be completely cured by thermal annealing at 300°C for ten hours. The γ-ray induced readout noise was estimated to be about 0.2 MeV and 1 MeV equivalent respectively in a radiation environment of 15 rad/h and 500 rad/h for LSO and LYSO samples of $2.5 \times 2.5 \times 20$ cm^3.

Figure 12 (Left) shows an expanded view of the longitudinal transmittance spectra for three samples before and after several steps of the γ-ray irradiation with integrated dose of 10^2, 10^4 and 10^6 rad. Also shown in the figure is the corresponding numerical values of the photo-luminescence weighted longitudinal transmittance ($EWLT$). Figure 12 (Right) shows the normalized average light output as a function of integrated dose for five long samples from various vendors. It is interesting to note that all samples show consistent radiation resistance

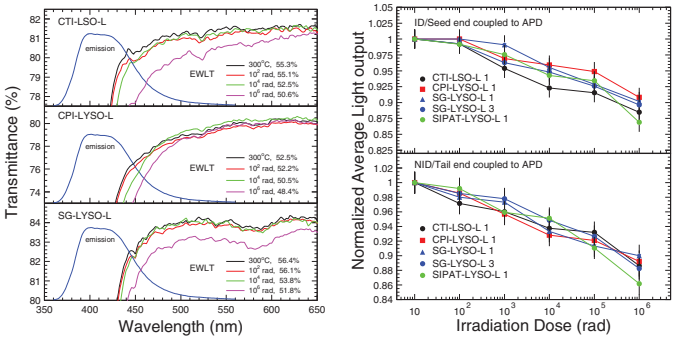

Fig. 12. Left: Transmittance spectra are shown as a function of wavelength in an expanded scale together with the photo-luminescence spectra for three long LSO and LYSO samples before and after the irradiation with integrated doses of 10^2, 10^4 and 10^6 rad. Right: Normalized light output with ID (top) and NID (bottom) end coupled to the readout device of two S8664-55 APDs is shown as a function of the integration dose for five long LSO and LYSO samples.

with degradations of both the light output and transmittance at 10 to 15% level after γ-ray irradiation with an integrated dose of 1 Mrad.

Assuming the same APD based readout scheme as the CMS $PbWO_4$ calorimeter, the expected energy resolution of an LSO/LYSO crystal based electromagnetic calorimeter would be

$$\sigma_E/E = \mathbf{2}\%/\sqrt{E} \oplus \mathbf{0.5}\% \oplus 0.001/E, \qquad (3)$$

which represents a fast calorimeter over large dynamic range with low noise. Such calorimeter would provide great physics discovery potential for high energy physics experiments in the proposed super B factory [16] as well as the proposed International Linear Collider (ILC) [17]. Because of its fast scintillation and good radiation hardness LYSO crystals are also proposed for the CMS $PbWO_4$ crystal endcap calorimeter upgrade at SLHC [18].

IV. Crystal Hadronic Calorimeter

Crystals have recently been proposed to construct a homogeneous calorimeter, including both electromagnetic and hadronic part [7]. This homogeneous hadronic calorimeter concept removes the traditional boundary between ECAL and HCAL, so eliminates the effect of dead materials in the middle of the hadronic shower development. It takes advantage of recently implemented dual readout approach to measure both Cherenkov and scintillation light to achieve good energy resolution for hadronic jets measurement [8]. Because of the un-precedent volume (70 to 100 m^3) foreseen for such calorimeter [7], the crystal material must be dense (to reduce the volume), UV transparent (to effective collecting the Cherenkov light) and allows a clear discrimination between the Cherenkov and scintillation light.

Figure 13 (Left) shows samples of three $5 \times 5 \times 5$ cm^3 crystal samples: PbF_2, BGO and PWO. Crystals of this size can be seen as typical building block for a crystal hadronic calorimeter. All material are dense (PbF_2 has of a density of 7.7 g/cm^3) with a nuclear interaction length about 22 cm. Mass production capability exists for all three candidate materials with cost among the lowest for materials of such density. Figure 13 (Right) shows the transmittance spectra of PbF_2 (green), BGO (blue), PWO (red) and a UG11 filter (black) as a function of wavelength together with the Cherenkov emission spectrum (dashed blue). The UG 11 filter can be used

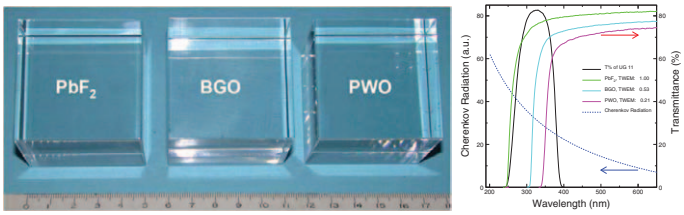

Fig. 13. Left: A photo shows three crystal samples of $5 \times 5 \times 5$ cm^3 investigated for the homogeneous hadronic calorimeter concept. Right: The transmittance spectra of PbF_2 (green), BGO (blue), PWO (red) and UG11 (black) are shown as a function of wavelength. Also shown in this figure are the Cherenkov emission spectrum (dashed blue) and the normalized figure of merit for the Cherenkov light measurement with the UG11 filter.

to select the Cherenkov light with small or no scintillation contamination. Also shown in this figure is the normalized figure of merit for the Cherenkov measurement (TWEM) by using the UG11 filter, which is defined as the transmittance weighted Cherenkov emission spectrum. Their numerical values are 1.0:0.53:0.21, which would be 1.0:0.82:0.75 without using the UG11 filter. Among these materials PbF_2 is the most effect in collecting the Cherenkov light because of its good UV transmission.

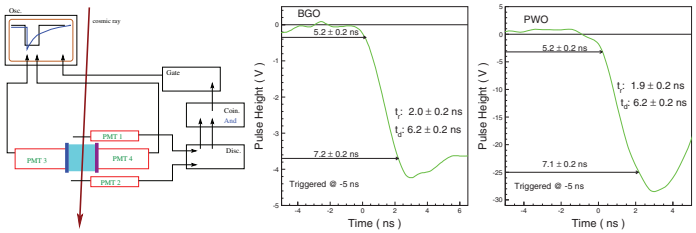

Fig. 14. Left: A schematic showing a simple set-up used to measure cosmic-ray generated Cherenkov and scintillation light simultaneously by using two Hamamatsu R2059 PMT. The light pulses are recorded by an Agilent 6052A digital scope. Digital scope traces of the scintillation light front edge measured by a Hamamatsu R2059 PMT with GG400 filter for the BGO (Middle) and PWO (Right) samples.

Effective discrimination between Cherenkov and scintillation light can be realized by using optical filter. Figure 14 (Left) shows a set-up used to investigate Cherenkov light collection and its separation from the scintillation light. Cosmic-rays were triggered by two finger counters with coincidence. The Cherenkov and scintillation light pulses generated by cosmic-rays were measured simultaneously by two Hamamatsu R2059 PMT coupled to the sample through optical filters UG11 and GG400. GG400 is a low-pass filter with cut-off at 400 nm. The UG11 filter is used to select the Cherenkov light as shown in Figure 13 (Right). The GG400 filter is used to select the scintillation light with small contamination of the Cherenkov light. The output of these two PMTs were digitized by an Agilent 6052A digital scope. Figure 14 (Middle and Right) shows the front edge of the scintillation light pulse from BGO and PWO, observed through the GG400 filter. Their delay from the trigger (t_d) and rise time (t_r) are identical with numerical values of 6.2 ns and 1.9 ns respectively. Figure 15 shows the Cherenkov light pulse shape observed for PbF_2 (Left), BGO (Middle) and PWO (Right) through the UG11 filter. All pulses have consistent time structure in the delay (6.1 ns), the rise time (1.8 ns), the fall time (4.2 ns) and the FWHM width (3.0 ns). It is interesting to note that there is no difference observed in the delay and rise time between the Cherenkov and scintillation light, indicating that only the light pulse width and fall time are useful for the discrimination between the Cherenkov and scintillation light. A slow scintillator may help this discrimination.

The ratio of Cherenkov versus scintillation light was measured to be 1.55% and 22% for BGO and PWO respectively. These values are consistent with the scintillation light yield shown in Table II, the emission weighed quantum efficiency of bi-alkali cathode of the Hamamatsu R2059 PMT shown in Figure 8 (Left) and the TWEM values shown in Figure 13

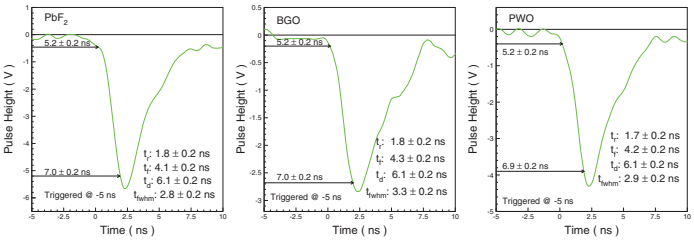

Fig. 15. Digital scope traces of Cherenkov light pulse measured by a Hamamatsu R2059 PMT with UG11 filter for the PbF_2 (Left), BGO (Middle) and PWO (Right) samples.

(Right).

Development of cost-effective material is crucial for the homogeneous hadronic calorimeter concept. While BGO is the best material to be used for such calorimeter, R&D is actively pursued by the high energy physics community for additional materials. One approach is to develop PWO crystals with slow scintillation emission . Green (560 nm) and slow emission with a few μsec decay time was observed by selective doping in PWO crystals [19]. Such crystals were reported to have a factor of ten more light than yttrium doped PWO crystals used in high energy physics experiment. This slow and green scintillation would be desirable for this application.

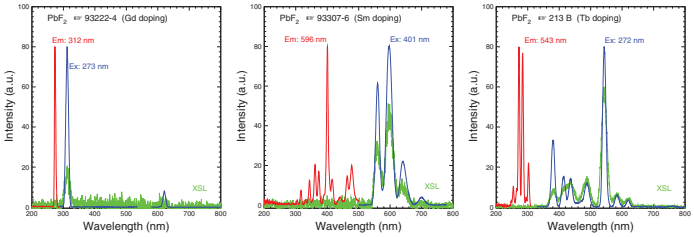

Fig. 16. UV excitation (red), photo-luminescence (blue)and x-luminescence (green) spectra are shown as a function of wavelength for Gd (Left), Sm (Middle) and Tb (Right) dopes PbF_2 samples.

Another approach is to develop scintillating PbF_2 crystals by selective doping. Observations of fast scintillation in Gd or Eu doped PbF_2 crystals were reported [20], [21]. Our investigation shows that rear earth doping introduces scintillation in PbF_2, but not in the level can be measured by using γ-ray source. Figure 16 show the excitation, photo-luminescence and x-luminescence spectra for Gd, Sm and Tb doped PbF_2 crystal samples. It is noted that the scintillation of Sm and Tb doped PbF_2 samples is between 500 to 600 nm, which is desirable for Cherenkov/scintillation discrimination. Investigation is continuing aiming at developing cost-effective materials for this concept.

V. Summary

Precision crystal electromagnetic calorimeters have been an important part of high energy physics detector. In addition to the Panda PWO electromagnetic calorimeter at Fair, the availability of mass production capability of large size LSO and LYSO crystals provides an opportunity to build a LSO/LYSO crystal electromagnetic calorimeter with unprecedent energy resolution over a large dynamic range down

to MeV level. Such calorimeter, if built, would greatly enhance the physics discovery potential for high energy and nuclear physics experiments in the next decade.

Recent interest in high energy physics community to pursue homogeneous hadronic calorimeter with dual readout opens a new area of crystal calorimetry to achieve good energy resolution for hadronic jets in the next decade. The main challenge for this concept is to develop cost effective heavy crystal scintillators with good UV transmission and excellent Cherenkov/scintillation discrimination.

REFERENCES

[1] G. Gratta, H. Newman and R.-Y. Zhu, *Annu. Rev. Nucl. Part. Sci.* **44** 453 (1994).

[2] E. Bloom and C, Peck, *Ann. Rev. Nucl. Part. Sci.* **33** (1983) 143-197.

[3] *The CMS Electromagnetic Calorimeter Project*, CERN/LHCC 97-33 (1997).

[4] R.-Y. Zhu, *Nucl. Instr. and Meth.* **A537** (2005) 344.

[5] U. Chaturvedi *et al.*, *Nucl. Instr. and Meth.* **A461** 376 (2001).

[6] P. Adzic *et al.*, "Energy Resolution of the Barrel of the CMS Electromagnetic Calorimeter," **JINST 2** P04004 (2007).

[7] A. Para, talk given in International Linear Collider Workshop 2008 at Chicago.

[8] R. Wigmans, in *Proceedings of VII International Conference on Calorimetry in Particle Physics*, Ed. E. Chen *et al.*, World Scientific (1998) 182, and N. Akchurin *et al.*, *Nucl. Instr. and Meth.* **A537** (2005) 537.

[9] C. Melcher, V.S. Patent 4958080 (1990) and 5025151 (1991).

[10] D.W. Cooke, K.J. McClellan, B.L. Bennett, J.M. Roper, M.T. Whittaker and R.E. Muenchausen, *J. Appl. Phys.* **88** (2000) 7360 and T. Kimble, M Chou and B.H.T. Chai, *2002 IEEE NSS Conference Record*.

[11] E. Loef, P. Dorenbos, E. Eijk, K. Kraemer and H. Guedel, *Nucl. Instr. and Meth.* **A486** (2002) 254.

[12] R.H. Mao, L.Y. Zhang and R.-Y. Zhu, *IEEE Trans. Nucl. Sci.* **NS-55** (2008).

[13] D.A. Ma and R.-Y. Zhu, *Nucl. Instr. and Meth.* **A333** (1993) 422.

[14] J.M. Chen, R.H. Mao, L.Y. Zhang and R.-Y. Zhu, *IEEE Trans. Nucl. Sci.* **54** (2007) 718.

[15] J.M. Chen, R.H. Mao, L.Y. Zhang and R.-Y. Zhu, *IEEE Trans. Nucl. Sci.* **54** (2007) 1319.

[16] SuperB Conceptual Design Report, **INFN/AE-07/2, SLAC-R-856, LAL 07-15**, March (2007).

[17] R.-Y. Zhu, *A LSO/LYSO Crystal Calorimeter for the ILC*, talk presented in 2005 ILC Workshop, Snowmass. http://nicadd.niu.edu/cdsagenda//fullAgenda.php?ida=a0561.

[18] R.-Y. Zhu, *Development of LYSO Crystals for CMS at SLHC*, talk presented in CMS ECAL SLHC Workshop, CERN. http://www.hep.caltech.edu/ zhu/talks/ryz_080415_SLHC.pdf.

[19] R.H. Mao *et al.*, in *Proceedings of IX International Conference on Calorimetry in Particle Physics*, Ed. B. Aubert *et al.*, Franscati Physics Series Vol. XXI (2000) 709-720.

[20] D. Shen *et al.*, *Jour. Inor. Mater.* **Vol 101** (1995) 11.

[21] C. Woody *et al.*, in *Proceedings of SCINT95*, Delft University Press, Delft, The Netherlands, (1996).

[22] Philippe Rosier, in these Proceedings.